2D Plasmonic Superlattice Based on Au Nanoparticles Self-Assembling Onto a Functionalized Substrate

ARTICLE *in* THE JOURNAL OF PHYSICAL CHEMISTRY C · MARCH 2014

Impact Factor: 4.77 · DOI: 10.1021/jp4126792

THE JOURNAL OF PHYSICAL CHEMISTRY C

Article

pubs.acs.org/JPCC

Two-Dimensional Plasmonic Superlattice Based on Au Nanoparticles Self-Assembling onto a Functionalized Substrate

Michela Corricelli,[†,‡] Nicoletta Depalo,[†] Elisabetta Fanizza,[†,‡] Davide Altamura,[§] Cinzia Giannini,[§] Dritan Siliqi,[§] Rosa Di Mundo,[‡] Fabio Palumbo,[⊥] Vasily G. Kravets,[∥] Alexander N. Grigorenko,[∥] Angela Agostiano,[†,‡] Marinella Striccoli,[†] and M. Lucia Curri*[,†]

[†]Istituto per i Processi Chimico Fisici (IPCF-CNR) Bari, c/o Dipartimento di Chimica and [‡]Dipartimento di Chimica, Università degli Studi di Bari, Via Orabona 4, Bari I-70126, Italy

[§]Istituto di Cristallografia (CNR-IC), Via Amendola 122/O, Bari I-70126, Italy

[⊥]CNR-IMIP, Istituto di Metodologie Inorganiche e Plasmi, Via Orabona 4, Bari I-70126, Italy

[∥]School of Physics and Astronomy, the University of Manchester, Manchester M13 9PL, United Kingdom

Supporting Information

ABSTRACT: Au nanoparticles (NPs) self-assembled by means of a simple solvent evaporation strategy in a two-dimensional (2D) superlattice with a highly controlled geometry and extending over micrometers squared when drop cast onto a suitably functionalized silicon substrate. The assembly procedure was defined by carefully monitoring experimental parameters, namely, dispersing solvent, deposition temperature, Au NP concentration, and chemistry of supporting substrate. The investigated parameters were demonstrated to play a significant role on the delicate energetic balance of the mutual NPs as well as NP−substrate interactions, ultimately directing the NP assembly. Remarkably, substrate surface chemistry revealed to be decisive to control the extent of the organization. Scanning electron microscopy demonstrated that the 2D superlattice extends uniformly over hundreds of square micrometers. Grazing-incidence small-angle X-ray scattering investigation validated the Au NP organization in crystalline domains and confirmed the role played by the surface chemistry of the substrate onto the 2D lattice assembly. Finally, preliminary spectroscopic ellipsometry investigation allowed extraction of optical constants of NP assemblies. The localized surface plasmon resonance modes of the NP assemblies were studied through a combined analysis of reflection, transmission, and ellipsometric data that demonstrated that the plasmonic properties of the Au NP assemblies strongly depend on the substrate, which was found to influence NP ordering and near-field interactions between NPs.

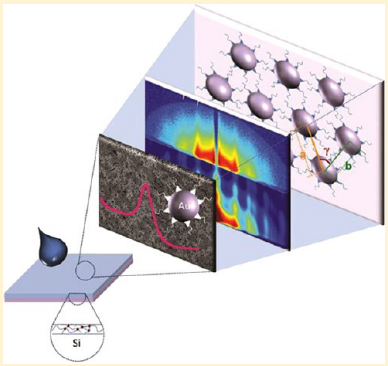

INTRODUCTION

Nanoparticle (NP) assemblies are emerging in modern material science as a new platform for bottom-up design of functional superstructures. Two-dimensional/three-dimensional (2D/3D) hierarchical organizations of NPs in superlattices represent ideal candidate structures for a wide range of technological applications, such as light-emitting devices,[1] biological tags,[2,3] catalysts,[4,5] and solar cells.[6,7]

Building blocks for fabricating such a class of superstructures can be obtained by suitably synthesizing and/or properly surface engineering previously prepared NPs. Their organization can be then externally driven by applying magnetic,[8] electric,[9] or flow fields,[10] as well as by capillary forces.[11] As an alternative, self-assembly represents a particularly simple and effective strategy. The self-assembly approaches rely on a delicate equilibrium of specific short-range interactions, such as dipolar forces and van der Waals interactions. It is generally accepted that minimization of these energy contributions is the driving force for the superstructure formation.[12] Spontaneous organization of such particles to form superlattices requires a high control on NP size and size distribution. Indeed, many parameters influence the formation and the extent of a superlattice such as NP concentration, dispersing solvent, and substrate. Also, capping agent chain length and composition, and for a binary superlattice, NP size and concentration ratio, can strongly affect the final geometry.[13]

NPs organized into ordered superlattices provide systems with properties that significantly differ from those of isolated NPs. The size-dependent characteristics of the individual components combine with the original collective properties that arise from the interactions between the nano-objects,[14] even where only a local NP order is present. Fabrication of superlattices starting from NPs with a suited composition offers a very promising and cost-effective approach to a large variety of functional materials. Their properties can be finely tuned not only by playing with chemical composition but mainly by

Received: December 27, 2013
Revised: March 4, 2014
Published: March 7, 2014

   dx.doi.org/10.1021/jp4126792 | J. Phys. Chem. C 2014, 118, 7579−7590

carefully controlling the mutual position of the components. For example, cascade energy transfer in structures made of layer-by-layer assembled CdTe nanocrystals (NCs) was realized by a funnel-like band gap profile, thus obtaining a system potentially useful for tunable lasers.[15] Moreover, in the case of close-packed PbS NCs, the energy coupling effectiveness between neighboring nano-objects was found to be dependent on both the interparticle distance and the NC size.[16] Increasingly, growing interest was recently directed to plasmonic metamaterials, a new class of artificial materials, which offer unique possibilities to manipulate light. Noble metal (e.g., Au and Ag) NPs with controlled geometry are good candidates as meta-atoms for a metamaterial. Their typical absorption and scattering properties in the visible and near-infrared regions are due to the localized surface plasmon resonances (LSPRs), which are collective oscillations of the metal NP surface electrons when interacting with light.[17] Recently, metal NPs were organized in dimers,[18] or alternatively, one-dimensional (1D),[19] 2D,[20] and 3D[21] arrays, revealing original collective plasmonic properties that were implemented in state-of-the-art optical structures, such as nanoplasmonics and plasmonic metamaterials. Also a near-field coupling between the surface plasmons of neighboring Au NPs was demonstrated, owing to the transfer and confinement of electromagnetic energy.[22] In addition, it was reported the existence of a phase relation between the vibrations of all the Ag NPs organized in a supracrystal.[23] In this perspective, the rational design of meta-atoms, that is, building blocks constituting the metamaterial, is of fundamental importance in order to tailor the electromagnetic response, ultimately resulting in unique properties, even not existing in the natural world, for example, effective negative refractive index.[24] So far, the fundamental control of electromagnetic response in metamaterials was mostly achieved through complex top-down fabrication techniques, such as ion beam lithography and electron beam.[25,26]

On the other hand, bottom-up strategies are also promising. Colloidal chemical approaches demonstrated particularly suited for achieving high-quality crystalline noble metal nanostructure, such as nanowires[27] and NPs,[23−26] that overcome the main drawbacks of the generally time-consuming and very expensive lithographic routes. In addition, such high-quality metal nanostructures allow reduction of the internal losses that are mostly related to the resistive ohmic damping (e.g., electron−electron scattering and electron−phonon scattering) as well as to scattering at surfaces, roughness, or defects of metal nanostructures.[28]

Here, the concept is to assemble via a "soft chemistry" solvent evaporation method colloidal noble metal NPs into ordered plasmonic superlattices, toward the fabrication of possible metamaterials. The assembly of Ag octahedral NPs, capped with polyvinylpyrrolidone, was reported to occur over areas of a few millimeters via slow evaporation and sedimentation. The process was found to be promoted by the polymer acting as a capping agent, directly affecting the crystallization process via repulsive steric interactions, and ultimately favoring the formation of the highly packed structure.[21] Thiol-capped Au NPs were assembled onto areas of the order of a few square centimeters, by combining the Langmuir−Blodgett technique with an air plasma treatment, in order to modify the layer wetting properties in between the deposition of two successive NP layers.[29] A 3D superlattice of 6.2 nm dodecanthiol-capped Au NPs was also reported.[30] However, only a few examples of 2D superlattices of Au NPs were presented.[31] Recently, a very large Au NP superlattice was realized at the water/toluene interface, in absence of ligand excess, being the supercrystal extent limited by the drop size.[32] The conductance of NP arrays was reported to be dependent on the conjugated oligomers used as capping molecule.[33] It was also reported that an integrated approach of structural (grazing-incidence small-angle X-ray scattering, GISAXS) and optoelectronic (photoconductance) investigations provided complementary insights into a nanoscale system made of Au NPs organized in a 2D array.[34]

Here, the formation of a 2D superlattice formed by solvent evaporation of oleylamine (OA)-capped Au NPs, self-assembling over hundreds of square micrometer areas when carried out on properly treated substrates, is reported. The influence of parameters such as evaporation temperature, NP dispersing solvent, NP concentration, and substrate surface chemistry was studied. Scanning electron microscopy (SEM) investigation clearly proved that increasing the solvent boiling point and drop casting temperature resulted in a higher tendency to organize according to a regular hexagonal geometry. However, once selected the optimal NP concentration, the chemical functionalization of the supporting substrate was found decisive to direct the overall assembly process over extended areas.

Morphological investigation proved that Au NP solution evaporation, carried out onto the prepared Teflon-like modified silicon substrates, turned out not only in a larger extent of the NP superlattice organization but also into an overall control of the final NP geometry. GISAXS investigation demonstrated that the surface chemistry induces different deviations from the regular hexagonal symmetry. Such features were explained in terms of chemical affinity between OA molecules capping NPs and the coating of the underlying substrate, namely, the native silica layer or alternatively the Teflon-like film. In particular, only negligible deviations from the regular hexagonal symmetry were found for the assemblies fabricated onto the Teflon-like coated substrate. A preliminary investigation of the optical properties of Au NPs assembled on the different substrates was also performed by means of spectroscopic ellipsometry, which allowed extraction of optical constants of NP assemblies. A combined analysis of reflection, transmission, and ellipsometry data revealed that the LSPR modes of the NP assemblies strongly depend on the substrate, which influences NP ordering and near-field interactions between NPs.

EXPERIMENTAL SECTION

Materials. Hydrogen tetrachloroaurate(III) trihydrate ($HAuCl_4{\cdot}3H_2O$, 99.999%), oleylamine (OA, technical grade 70%), and solvents hexane, toluene, and nonane (of the highest purity available) were purchased from Sigma Aldrich and were used without further purification.

Au NP Synthesis and Characterization. Spherical OA-coated Au NPs were prepared by following a versatile reported method with minor modifications.[35,36] In a typical experiment, OA was heated at 130 °C under vacuum and purified prior to use. A mixture of Au precursor, namely, tetrachloroauric acid ($HAuCl_4{\cdot}3H_2O$, 60 mg), and OA (1.3 g) was dissolved in toluene (1 mL) and injected into a three naked flask containing a refluxing solution of OA (2.5 g) in 49 mL of toluene. The OA acts both as a reducing agent during the NP growth and a coordinating molecule at the end of the synthesis. Upon injection and heating at high temperature (100 °C), the

dx.doi.org/10.1021/jp4126792 | J. Phys. Chem. C 2014, 118, 7579−7590

reaction mixture color changes from orange to bright yellow, becoming then colorless, due to reduction of Au(III) to Au(I) and gradually turns into deep red, indicating the formation of Au NPs. The particle growth was monitored by absorption spectroscopy, and the reaction was stopped after two hours. The as-prepared colloidal dispersion in toluene was first centrifuged in order to remove larger metal particle aggregates and then used for a subsequent Au NP size sorting treatment, which was carried out in order to improve the Au NP size distribution. Such a treatment consisted in addition of methanol (1.5 mL) to the NP dispersion (6 mL). Upon centrifugation at 950*g* for 10 min, the NPs were precipitated, collected, and redispersed in organic solvent (toluene or nonane). The NP concentration was obtained by calculating the extinction coefficient of OA-capped Au NPs in toluene, according to the approach described by Liu et al.[37]

The absorption spectra of Au NPs were recorded on samples purified and redispersed in toluene or nonane, by means of a Cary Varian 5000 UV−visible−near-IR (UV−vis−nIR) spectrophotometer. Transmission electron microscopy (TEM) analyses were performed by using a Jeol-Jem 1011 microscope, working at an accelerating voltage of 100 kV. TEM images were acquired by a Quemesa Olympus CCD 11 Mp camera. The samples for TEM investigation were prepared by dipping the 300 mesh carbon-coated Cu grid in the toluene or nonane solution of Au NPs. The solvent was allowed to evaporate before the analyses. Size statistical analysis (NP average size and size distribution) of the samples was performed by the freeware ImageJ analysis program. In particular, the average NP size and the percentage relative standard deviation ($\sigma_{\%}$) were calculated for each sample, providing information on NP size distribution.

Teflon-like Film Deposition and Characterization. Deposition of Teflon-like films was carried out in a radio-frequency (13.56 MHz) parallel plate plasma reactor fed with hexafluoropropene (C_3F_6) and argon as gas buffer, according to a previously reported procedure.[38,39] High Ar to monomer flow rate ratio and high discharge power were reported to produce Teflon-like films characterized by a high cross-linking degree. The experimental parameters employed in this work (Table 1)

Table 1. Experimental Conditions Used for the Realization of the Two Different Teflon-like Films

	Si/TL_	Si/TL$_+$
C_3F_6 flow rate	20 sccm	20 sccm
Ar flow rate	10 sccm	20 sccm
pressure	200 mTorr	200 mTorr
discharge power	200 W	250 W

allowed functionalization of silicon with Teflon-like films characterized by different cross-linking degree. We will refer as to Si/TL_ and Si/TL$_+$ for the silicon coated by the Teflon-like film with lower and higher cross-linking degree, respectively.

The Teflon-like film thicknesses were measured by means of an Alpha-Step D-120 Stylus profiler (the step was created by scratching the deposited film). Field emission scanning electron microscopy (FE-SEM) measurements were performed by means of a Zeiss Sigma microscope operating in the range 0.5−20 kV. Samples were set onto stainless-steel stub sample holders, by double-sided carbon tape. When measurements were carried out on silicon substrates functionalized with Teflon-like films, the samples were also grounded with silver paste. Topography atomic force microscopy (AFM) micrographs were recorded in tapping mode, on Si/TL_ and Si/TL$_+$ substrates, by using a PSIA XE-100 SPM system operating in air and at room temperature. A high frequency silicon cantilever for noncontact/tapping mode made by NanoWorld was used. Micrographs were collected by sampling the surface at a scan rate of 0.5−1.0 Hz, with a resolution of 256 × 256 pixels and scan area of 2 × 2 μm^2. AFM images were processed by using the XEI program. A CAM200 digital goniometer (KSV instruments) equipped with a BASLER A60f camera was used to evaluate the advancing and receding water contact angle (WCA) of the surface of substrates. A maximum droplet volume of 3 μL was used for these measurements. X-ray photoelectron spectroscopy (XPS) analysis was carried out with a Thermo Electron Corporation Theta Probe spectrometer using a monochromatic Al Kα X-ray source (1 486.6 eV) at a spot size of 400 mm corresponding to a power of 100 W at a takeoff angle of 38. Survey (0−1 200 eV) and high-resolution spectra (C1s, O1s, F1s) were recorded at a pass energy of 200 and 150 eV, respectively. The C1s signal for C−C(H) bonds, with a binding energy of 284.7 eV, was used as an internal standard for the correction of the samples charging. The elemental analysis was calculated by using the sensitivity factors of the instrument from the high resolution peaks.

Au NP Self-Assembly. Au NPs were organized onto 1 cm × 1 cm supporting substrates, by means of a drop-casting procedure. Briefly, 30 μL of Au NP solution, with a concentration equal to 4 × 10^{-7} M or alternatively 8 × 10^{-7} M were drop-cast onto silicon coated by a native layer of silicon oxide (Si/SiO_2), Si/TL_ and SI/TL$_+$, respectively. The solvent was let to evaporate in open-air conditions and keeping the substrate horizontal. The temperature was carefully controlled by means of a hot plate.

GISAXS measurements were performed by using a Rigaku S-MAX3000 SAXS/WAXS system[40] equipped with a Fr-E+ SuperBright rotating copper anode microsource (λ = 0.15405 nm). An X-ray beam spot size at a sample position of approximately 0.3 × 0.3 mm^2 (beam divergence 0.5 mrad) was adopted. A Triton20 gas-filled proportional counter, with 1024 × 1024 array and 195 μm pixel size, was used for data collection. The sample to detector distance was 2080 mm. Sample surface was aligned by means of a remote controlled goniometer stage with piezoelectric motors providing subarc-second precision.

Investigation of Optical Properties of NP Assembly. Resonant properties of plasmonic nanostructures were investigated by spectroscopic ellipsometry. Spectroscopic ellipsometry records optical spectra with a higher accuracy than absorption spectroscopy and allows extraction of optical constants of the prepared samples.[41] The optical measurements were performed with a J.A. Woollam ellipsometer in the 240−1000 nm wavelength range. A typical spot size was about 1 mm in nonfocusing mode and 30 μm in focusing mode. We acquired the spectra of the ellipsometric reflection $\rho = r_p/r_s = \tan(\Psi)\exp(-i\Delta)$ where r_p and r_s are the complex reflection coefficients for p and s polarized light, respectively, and (Ψ, Δ) are the ellipsometric angles. Both functions Ψ and Δ strongly depend on the optical properties of investigated samples, thus allowing extraction of optical constants for investigated layers. The fitting of the ellipsometry data was performed using Woollam WVASE32 software in which the complex refractive index can be extracted using a procedure based on a Fresnel multilayer model that minimizes the mean square error

dx.doi.org/10.1021/jp4126792 | J. Phys. Chem. C 2014, 118, 7579−7590

between the model and experimental data. A combined analysis of the reflection, transmission, and ellipsometry data of the sample was performed in order to carefully identify LSPR modes of assembly of Au NPs.

RESULTS AND DISCUSSION

Spherical OA-capped Au NPs were assembled by means of a solvent evaporation procedure. Highly monodisperse Au NPs were successfully prepared by combining the versatile synthetic strategy with an effective postpreparative size sorting procedure, based on an antisolvent (methanol) centrifugal fractional precipitation. The TEM micrograph (Figure 1a) and the related size distribution histogram (Figure 1a, inset) show that the average diameter of the size-sorted Au NPs is 11.7 ± 0.7 nm ($\sigma_{\%}$ = 6%), confirming the NP very narrow size distribution. Figure 1b reports the UV−vis absorption spectra of Au NPs when toluene and nonane are used as dispersing solvent, respectively. They both display the characteristic LSPR band in the visible region, although a slight shift in the peak maxima wavelength can be observed. Such an occurrence is accounted for by the different solvent refractive index, which is known to influence the LSPR wavelength.[42] The OA-capped Au NPs were successfully assembled by means of a solvent evaporation procedure. This procedure, although simple, requires a careful control of experimental parameters, such as solvent composition, temperature, and NP concentration, involved in the delicate equilibrium between distinct energetic contributions, such as entropic, van der Waals, steric, and dipolar forces.

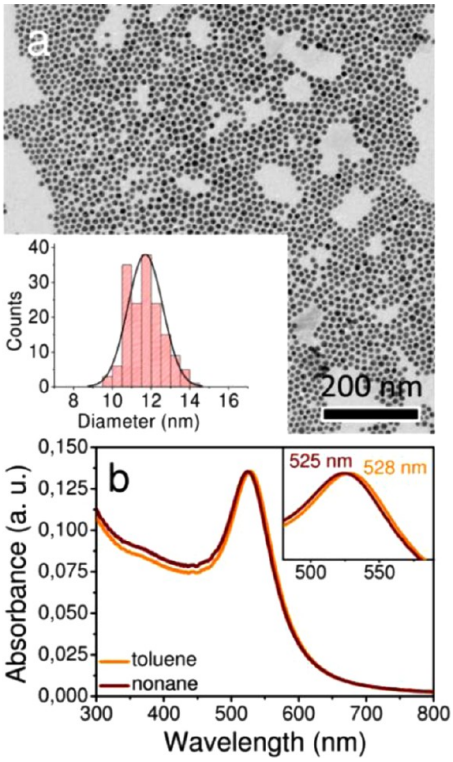

Figure 1. (a) TEM micrograph of the Au NPs and corresponding size distribution calculated from the TEM micrographs (inset). (b) UV−vis absorption spectra of the Au NPs in toluene (orange line) and nonane (purple line). Inset: magnification of the LSPR peaks.

Influence of Solvent, Temperature, and NP Concentration. In order to study the influence of the solvent on the NP organization, Au NPs in different solvents were drop-cast on silicon substrates. The dispersing solvent plays a crucial role in the NP final organization for two main reasons: (i) the vapor pressure, hence the boiling point, defines the time available for the particles to assembly in the most energetically favorable position;[43,44] (ii) the solvent polarity contributes to mediate the OA-capped Au interparticle interactions. Indeed, low relative electric permittivity values promote the occurrence of attractive interactions, while higher values are responsible of repulsive interactions between the Au NPs. In a previous work, oleic acid-capped PbS NCs have been demonstrated to experience interparticle attractive interactions when dispersed in a low permittivity solvent, thus forming regular structures.[43,45] The occurrence of attractive or repulsive interactions depends both on the solvent and the organic molecule capping the NCs.[45] Here, Au NPs represent a very similar system, since they are capped by OA molecules, having the same aliphatic chain of the oleic acid. However, such a type of interaction represents only a contribution in the delicate equilibrium regulating the formation of a superlattice. Here, three solvents, namely, hexane, toluene, and nonane, all characterized by relatively low relative electric permittivity values (1.9, 2.4, and 2.0, respectively)[46] were used to disperse the Au NPs, in order to study the influence of the solvent vapor pressure on the overall assembly and at same time guarantee the occurrence of attractive interactions. Hexane, toluene, and nonane are characterized by increasing boiling points, equal to 69, 111, and 151 °C, respectively.[46]

This resulted in NP assemblies with different morphology, as shown by the SEM micrographs reported in Figure 2a−c. Namely, Au NPs appear only randomly organized when hexane is used as dispersing solvent, while small areas of hexagonally packed Au NPs are visible when they are deposited from toluene and nonane. The amount and the extent of the regularly arranged domains were seen to significantly increase passing from toluene to nonane, thus clearly pointing out the influence of the solvent vapor pressure on the overall NP organization. Indeed, increasing the solvent boiling point, longer evaporation times can be experienced by the NPs that can thus take advantage for finding the energetically most favored position.[43,44] The effect of temperature was then tested by drop-casting 30 μL of 4 × 10^{-7} M Au NPs in nonane solution onto Si/SiO_2 substrate and leaving the solvent evaporate at 40 °C, by using a hot plate (Figure 2d). SEM micrograph of the obtained NP assembly confirmed a hexagonal geometry for the assembly and clearly indicated that the increase in temperature led to the formation of larger NP areas (a few hundreds of nm^2). Such an evidence is consistent with the fact that an increase in NP mobility, occurring at higher temperature, allows them to find an energy minimum in the process.

However, a further increase in temperature (90 °C) resulted detrimental for the resulting assembly. In fact, the SEM micrograph in Figure 2e shows only a few hexagonally organized areas alternated to randomly organized zones. In addition, contamination deriving from organic matter can be observed, due to a partial segregation of Au NP capping molecules (OA) desorbed at such a temperature. Finally, the effect of NP concentration was tested, by increasing it from 4 × 10^{-7} to 8 × 10^{-7} M. In Figure 2f, the SEM micrograph clearly shows that such an increase in NP concentration turns in the

dx.doi.org/10.1021/jp4126792 | J. Phys. Chem. C 2014, 118, 7579−7590

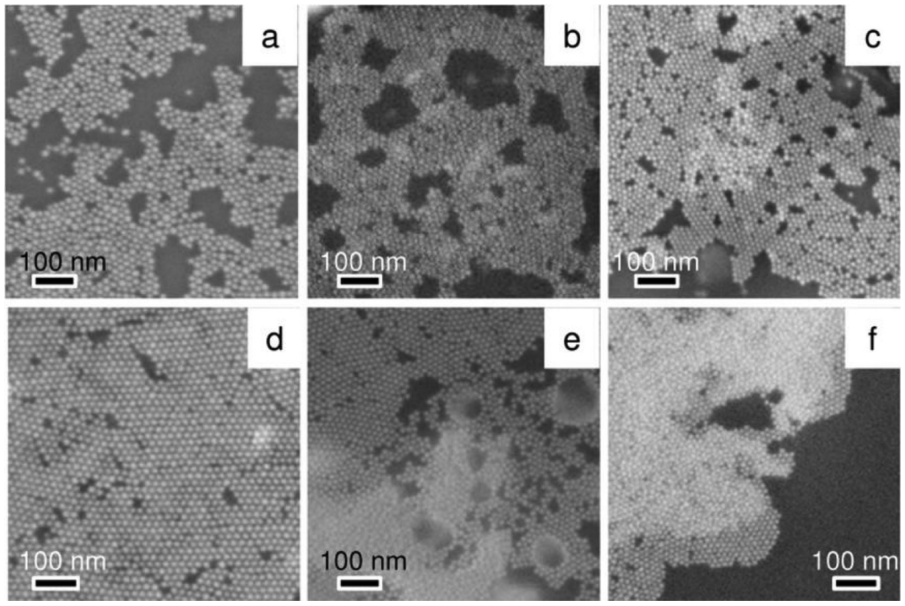

Figure 2. SEM micrographs of the structure resulting from drop-casting 30 μL of 4×10^{-7} M Au NP solution in (a) hexane, (b) toluene, and (c) nonane at room temperature on Si/SiO_2 substrates. Drop-cast structures obtained from 30 μL of 4×10^{-7} M Au NP nonane solution at (d) 40 °C and (e) 90 °C and 30 μL of 8×10^{-7} M Au NP nonane solution at (f) 40 °C.

formation of an island of multilayered NPs alternated to empty areas. Such features can be explained by considering that Au NPs prefer to maximize their mutual interactions and reduce contact with the substrate, thus depleting some areas. In fact, a silicon substrate, handled in normal conditions, is coated by a native thin layer of SiO_2, which has a marked polarity, while OA molecules coordinate the NP surface with their polar heads, exposing their apolar long alkyl chains. Such a low chemical affinity accounts for the preference of NPs to mutually interact rather than uniformly distribute onto the SiO_2 film coating the substrate.

Effect of Substrate Surface Chemistry. The reported experiments demonstrated that, upon solvent evaporation, Au NPs tend to minimize the contact area with the silicon substrate, coated by a thin layer of SiO_2. Therefore, in order to overcome the low chemical affinity between the polar SiO_2 surface and the hydrophobic alkyl chain of OA molecules coordinating the NP surface, silicon substrates were functionalized.

Particularly, a thin Teflon-like coating was deposited via a cold plasma process, in order to modify the substrate surface chemistry. In Table 1, the experimental conditions used for fabricating the Teflon-like films at different degrees of polymer cross-linking are reported. High argon-to-monomer flow rate and at the same time high discharge power are known to typically bring to the formation of films with a high cross-linking degree, as a consequence of a stronger fragmentation of the precursor in the plasma and a more energetic ion bombardment at the surface.[38,39] Furthermore, impinging ions can transfer enough energy to the surface to activate bond formation between the sticking reactive film precursors and silicon atoms, thus enhancing the adhesion of the growing film with the substrate.

In particular, conditions potentially leading to a different extent of the Teflon-like cross-linking were investigated, thus obtaining two different substrates, Si/TL_- and Si/TL_+, referring to silicon coated by the Teflon-like film with lower and higher cross-linking degree, respectively. A different film thickness was measured by means of a profilometer for the two substrates, namely, of 100 and 50 nm for the Si/TL_- and Si/TL_+, respectively. Substrate surface topography was investigated by means of SEM and AFM. SEM micrographs (Figure 3a, b) show an almost flat surface, uniform over a surface tens of square micrometers, for both Si/TL_- and Si/TL_+ films.

AFM micrographs of silicon substrates functionalized with both Si/TL_- and Si/TL_+ films (Figure 3c, d) confirm a quite regular surface morphology. The topography was further proven by the corresponding roughness profiles (Figure 3c,

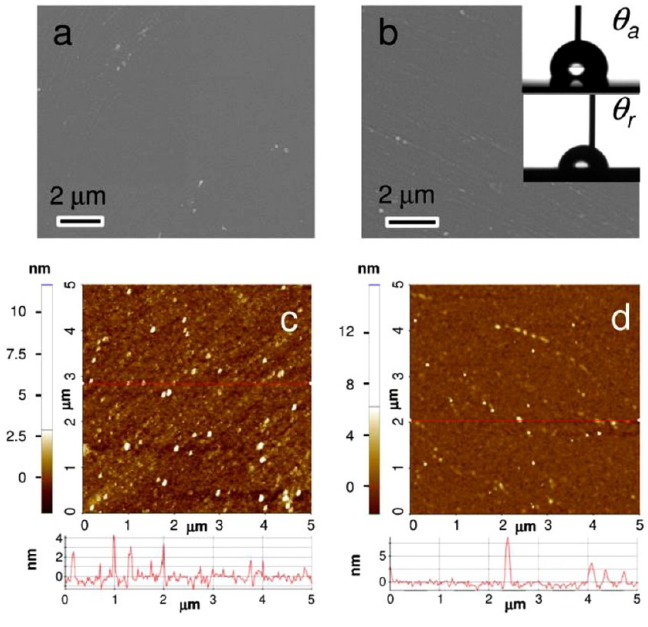

Figure 3. SEM and AFM micrographs and roughness profile with the corresponding average roughness, as obtained from AFM measurements, for Si/TL_- (left) and Si/TL_+ (right) films. Picture of the advancing (θ_a) and receding (θ_r) WCA measurements for the Si/TL_+ substrate (b, inset).

dx.doi.org/10.1021/jp4126792 | J. Phys. Chem. C 2014, 118, 7579−7590

d) and average roughness, which was found to be 0.6 and 0.7 nm in the case of Si/TL_ and Si/TL$_+$, respectively. The absence of significant changes in the surface topography after the plasma treatment clearly demonstrates a flat morphology. This is a strict requirement for achieving a reliable self-assembling procedure, which would be otherwise affected by the underlying substrate geometry.

WCA measurements were carried out on Si/TL_ and Si/TL$_+$ substrates and here shown for Si/TL$_+$ (Figure 3b, inset). The corresponding advancing (θ_a) and receding (θ_r) WCA values are displayed in Table 2. For comparison purposes, also the corresponding values for the bare Si/SiO$_2$ substrate were reported. After the Teflon-like film deposition, for both deposited films, an increase of both θ_a and θ_r was measured, with respect to bare Si/SiO$_2$, thus confirming that the Teflon-like coating increases the hydrophobic character of the surface. Indeed, as it can be easily inferred from the Young equation[47] and experimentally demonstrated,[48] hydrophobic materials have a lower wettability than hydrophilic ones, irrespectively from the solvent polarity, when the WCA measurement is carried out in air.

Table 2. Summary of Film Thickness, Obtained from Profilometer Measurements, Advancing and Receding WCA Values as Found in Literature for the Bare Si/SiO$_2$ Substrate[49] and Experimentally Measured for Si/TL_ and Si/TL$_+$, and Mean Roughness Obtained from AFM Measurements

	Si/SiO$_2$	Si/TL_	Si/TL$_+$
film thickness	–	100 nm	50 nm
θ_a (deg)	57 ± 1	117 ± 5	118 ± 5
θ_r (deg)	42 ± 1	90 ± 5	87 ± 5
mean roughness	–	0.6 nm	0.7 nm

However, the Teflon-like film deposition led to a higher mutual chemical affinity between the substrate surface and the apolar OA-capped Au NPs, thus in principle offering an additional parameter to drive the NP assembly, during the solvent evaporation.

XPS measurements were carried out on the Teflon-like coated silicon substrates, in order to study the chemical composition of the films (Figure 4). No significant difference is found in XPS atomic percentages between the Si/TL_ and Si/TL$_+$ Teflon-like films (Table 3). The shape of the C1s signal is quite similar in the two cases, and a similar distribution of fluorinated groups can be assumed. As expected, not a conventional Teflon coating is obtained but a fluorocarbon coating with a more complex structure. In particular, both C1s spectra indicate the presence of ending and propagating chain groups such as CF_3 and CF_2, respectively, and others that usually point out to the formation of branching and cross-linking, CF and C–CF. Hence, notwithstanding the different plasma conditions investigated, the obtained coatings show a very similar chemical composition and wettability behavior.

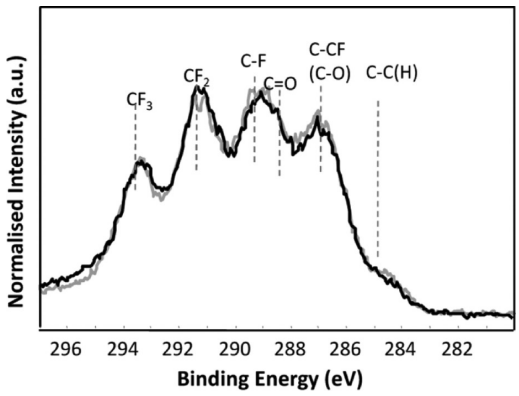

Figure 4. C1s XPS spectra of silicon coated with the Si/TL_ (gray) and Si/TL$_+$ (black) Teflon-like film, performed immediately after the film deposition.

Table 3. Atomic Content of Oxygen, Fluorine, and Carbon in Teflon-like Films, as Obtained from XPS Measurements

	Si/TL_	Si/TL$_+$
O%	3.3	2.8
F%	51.8	52.4
C%	44.9	44.8

The influence of the substrate chemistry on the NP organization was then investigated, taking into account the previously defined optimized drop-casting conditions. Namely, 30 μL of Au NP nonane dispersion (4×10^{-7} M) was drop-cast at 40 °C on Si/SiO$_2$ (Figures 2d and 5a), on Si/TL_ (Figure 5b, c) and Si/TL$_+$ (Figure 5d), respectively. Upon Au NP exposure, the Si/TL_ film seems to undergo to swelling (Figure 5c and Figure S1, Supporting Information), probably because of a low chemical resistance of the film due to a contemporary effect of nonane and temperature. In addition, even looking at the unswollen regions, Au NPs appear only randomly assembled (Figure 5b). However, when the Au NP solution was drop-cast on the Si/TL$_+$ substrate, a completely different behavior is observed (Figure 5d and Figure S1, Supporting Information). Indeed, the NPs organize with a hexagonal arrangement in monolayers over a very large area, of the order of hundreds of square micrometers as reported also in Figure S1 (Supporting Information). In this case, the film results resistant against swelling. This result is quite interesting, since it highlights that, even if the surface chemical composition of the two deposited coatings is very close, the TL$_+$ film has a higher stability in contact with the organic solvent. This can be explained with the harsh plasma conditions used, as higher power and monomer dilution in Ar have been widely demonstrated to lead to denser and more cross-linked coatings.

However, as XPS and WCA techniques probe surface thickness for approximately 2–5 nm depth, their results cannot properly account for differences occurring in the deeper region of the coatings, which can possess then different structure and hence different solvent resistance. Furthermore, it should be considered that the higher energy input in the TL$_+$ plasma deposition process can enhance binding of the sticking film precursors to the substrate thus promoting higher film adhesion, playing a role in the solvent resistance of the coating.

The fast Fourier transform (FFT) indicates that the degree of order increases passing from the Au NP assembly on Si/SiO$_2$ to Si/TL_ and then to Si/TL$_+$. In addition, in the last two cases, the spots present in the FFT are consistent with a hexagonal geometry of the superlattice, in accord with SEM observations.

GISAXS is a surface sensitive technique suitable to determine both the NP shape and the lattice unit cell parameters of NPs organized in regular 2D lattices. GISAXS investigation was performed in order to gain statistical information on the structure of the NP assemblies, averaged over large sample areas. In Figure 6, the GISAXS experimental (d–f) and

dx.doi.org/10.1021/jp4126792 | J. Phys. Chem. C 2014, 118, 7579–7590

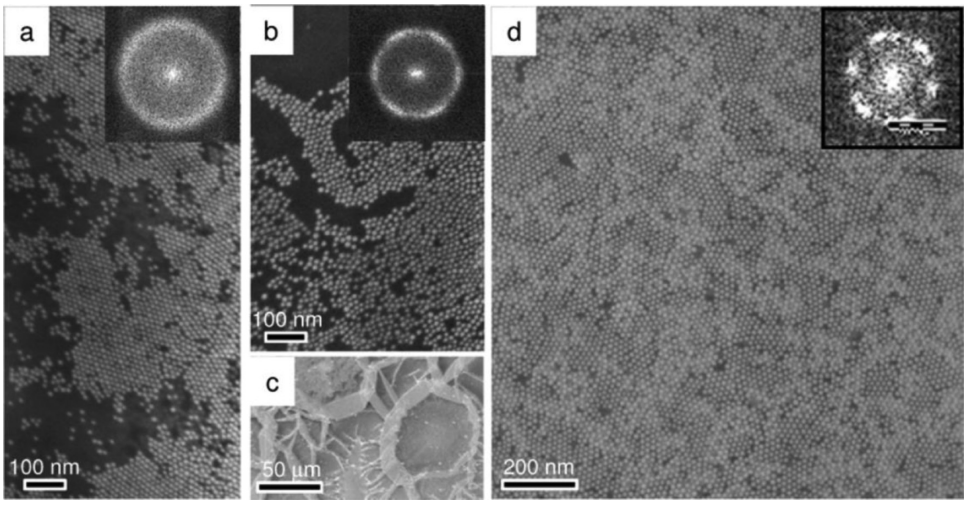

Figure 5. SEM micrographs of 4×10^{-7} M Au NPs in nonane drop-cast on the different substrates: (a) bare Si/SiO_2, (b, c) Si/TL_- at different magnifications, and (d) Si/TL_+, with the corresponding FFT.

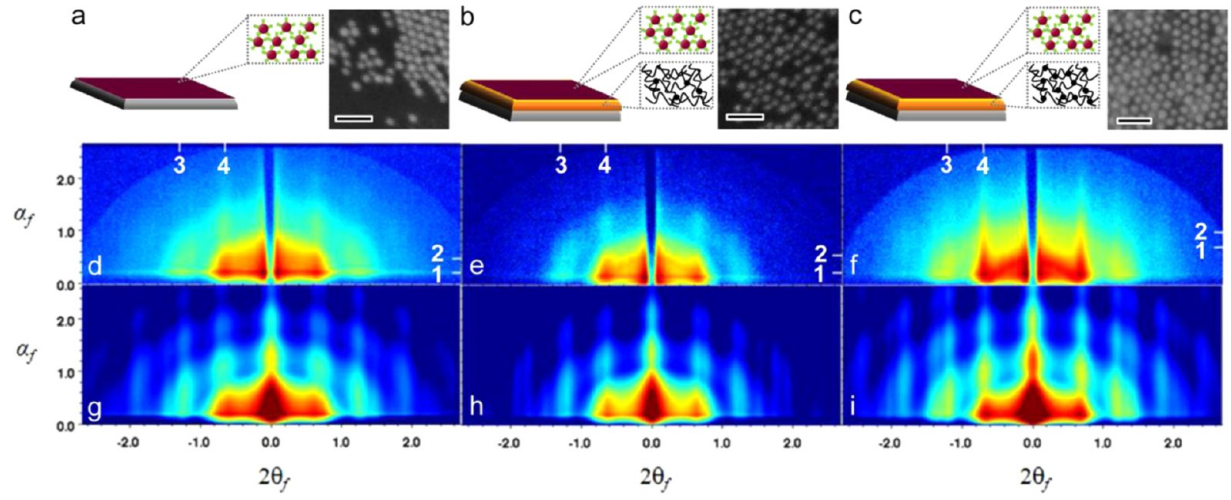

Figure 6. Scheme and SEM close-up (scale bar = 50 nm) of the Au NP self-assemblies, realized onto (a) Si/SiO_2, (b) Si/TL_-, and (c) Si/TL_+. Corresponding GISAXS (d–f) experimental and (g–i) simulated 2D maps.

calculated (g–i) maps recorded on the assemblies obtained by depositing NP dispersion onto the three differently functionalized substrates (Si/SiO_2, Si/TL_-, and Si/TL_+), corresponding to the SEM micrographs of Figure 5, are reported. The maps were collected with an incidence angle of the X-ray beam nominally of 0.28°.

A fitting procedure was used here to fully reproduce the 2D GISAXS patterns by using the IsGISAXS software.[50] Simulations and fits were performed in the Distorted Wave Born approximation, computing the total scattered intensity as the sum of four terms involving the direct scattering from the NPs (as in the Born approximation), a reflection from the substrate surface followed by scattering by the particle, and vice versa, reflection from the substrate surface followed by scattering by the particle and subsequent further reflection from the substrate. For a detailed description of GISAXS and its experimental applications, the reader may refer to refs 51 and 52, respectively.

Figure 7 reports the 1D profiles (panels a and b) extracted along the horizontal and vertical lines marked by the white ticks in Figure 6 and numbered accordingly. The experimental and calculated data in the 1D cuts of Figure 7a, b are shown as blue dots and a red line, respectively. The 2D maps are reported as a function of the exit angles parallel and perpendicular to the substrate, $2\theta_f$ and α_f, respectively, whereas the 1D cuts are reported as a function of the parallel and perpendicular components of the scattering vector (Q_y and Q_z, respectively), for completeness. A good agreement was obtained between calculated and experimental data for all samples, although small discrepancies can still be observed on the small-angle side, which are attributed to refraction/absorption effects in the NP layer. Such effects were taken into account in the simulations by considering the Au NPs as embedded in an effective layer, which allows data analysis with reasonable calculation times and reliable results (as confirmed by TEM and SEM analyses), contrary to the rigorous description given by the graded interface model.[51,53]

The fit of the complex refractive index (δ_L and β_L being its real and imaginary parts, respectively) in such an effective layer reveals a good agreement between calculation and experiment. In addition, similar values of δ_L ($4.0 \div 5.0 \times 10^{-6}$) and β_L (1.25×10^{-6}) were derived for all samples, namely, Au NPs assembled onto Si/SiO_2, Si/TL_-, and Si/TL_+; thus, it can be concluded that δ_L and β_L are actually related to the NP layer

dx.doi.org/10.1021/jp4126792 | J. Phys. Chem. C 2014, 118, 7579–7590

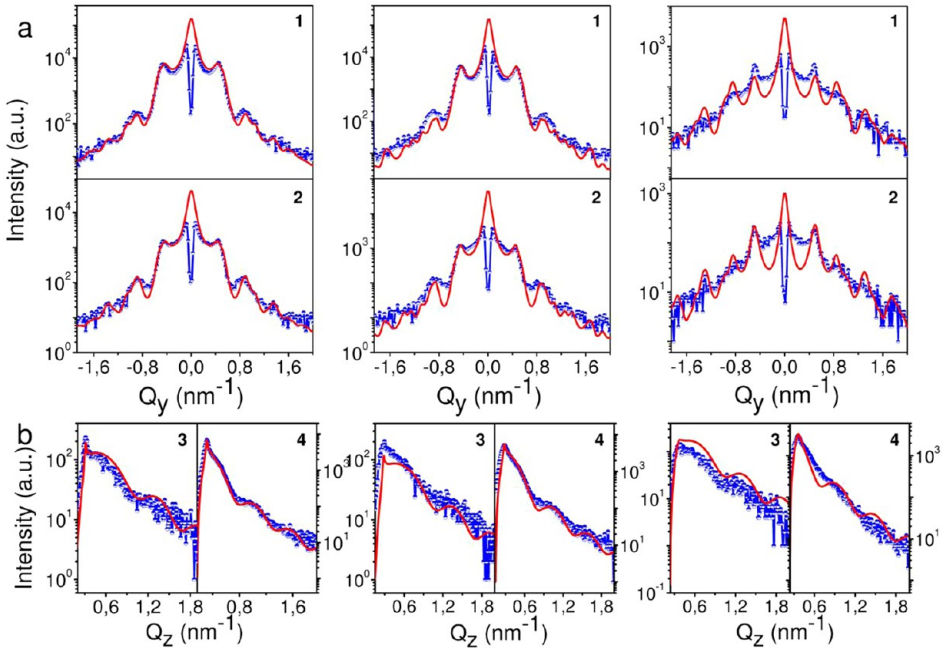

Figure 7. GISAXS experimental (dotted line) and calculated (solid line) 1D profiles extracted along the directions of the white ticks drawn on the 2D maps of Figure 6, correspondently labeled (horizontal-cuts at positions marked 1, 2; vertical cuts at positions marked 3, 4).

itself, irrespectively from the properties of the underlying substrate.

On the other hand, the scattering contribution of the supporting substrate was taken into account by assuming an effective average refractive index for the substrate, being this either bare Si or Teflon-like film coated Si. Such an approach is justified by the fact that the Teflon-like layer is several tens of nanometers thick, so that the thickness (Kiessig) fringes[51] are close enough not to significantly influence the overall behavior of the scattering intensity profile from the NP assembly. The average complex refractive index of the Si/$TL_{\pm}$ substrates was included as a fit parameter as well, although found not to significantly affect the calculated patterns, except for q_z values close to the Yoneda peak (~0.3 nm^{-1}, see Figure 7b).[51] For all the investigated substrates, good agreements between calculation and experiment were obtained. In particular, different average refractive index values were found for the different substrates, as expected. However, considering the model used, the obtained values should be only considered indicative ones. In fact, compared to the coefficients for the bare Si substrate ($\delta_{Si} = 7.58 \times 10^{-6}$; $\beta_{Si} = 1.73 \times 10^{-7}$), only a slight difference in the real part of the refractive index was derived for the TL_- film ($\delta_{Si/TL_-} = 6.8 \times 10^{-6}$); that is, the value for Teflon bulk material fits well, whereas larger differences were found in the case of the TL_+ film ($\delta_{Si/TL_+} = 4.3 \times 10^{-6}$; $\beta_{Si/TL_+} = 1.7 \times 10^{-6}$), probably due to its higher cross-linking degree.

Also, the apparently larger discrepancy observed in the 1D horizontal cuts (cut no. 1 in particular) for the NP assembly formed on the Si/TL_+ is due to the larger measured scattering intensity in the central region of the pattern, which is however due to the diffracted beam transmitted through the edge of the sample and not to the reflected scattered beam relevant to the GISAXS signal.

The fits allow inferring that the NPs are spherical in shape and 12 ± 1 nm in diameter, in agreement with TEM observations, and form in general 2D distorted hexagonal lattices with slightly different basis vector length (which correspond to interparticle center-to-center distance). Moreover, several superlattice domains with different orientations in the substrate plane exist within each assembly. The average structural parameters (basically the lengths a and b of the two basis vectors and the angle γ between them) deduced from the GISAXS fitting procedure are described in the following.

In the case of NPs directly deposited on Si/SiO_2 substrate, it was found that a = 14.0 ± 0.5 nm and b = 15.0 ± 0.5 nm, forming an angle of $\gamma = 70° \pm 2°$.

In the case of Au NPs deposited on the Si/TL_- substrate, from the GISAXS fit, it can be deduced that NPs form a distorted hexagonal lattice with $a = b$ = 15.0 ± 0.5 nm basis vectors, forming an angle $\gamma = 50°$ on average, possibly taking on larger values, up to 65°. The same kind of distortion of the hexagonal symmetry is therefore observed as in the case of NPs directly deposited on Si/SiO_2 substrates, although to a less extent.

Nevertheless, both distorted and regular hexagonal domains can be expected occurring in the samples, also having slightly different lengths of a and b vectors, giving rise to the multiple peaks in the horizontal GISAXS scans (panel a), in particular around 0.85 nm^{-1}. The peak around 1.1 nm^{-1} in particular is related to nonregular hexagonal symmetry ($\gamma \neq 60°, 120°$).

On the other hand, the assembly deposited on the Si/TL_+ substrate exhibits a slighter distortion with respect to the ideal hexagonal symmetry ($\gamma = 60°$), as the average value of the γ angle between the basis vectors is closer to 60°, being 57° and 63° the γ values that lead to better agreement between experimental and calculated data; a and b vectors still have slightly different average lengths, equal to 15.0 ± 0.5 and 14.5 ± 0.5 nm, respectively, although their range of values overlaps. GISAXS pattern is therefore more compatible in this case with the regular hexagonal symmetry.

As a result, the symmetry of the assemblies formed on Si/SiO_2, Si/TL_-, and Si/TL_+ substrates is therefore generally described by a (2D) oblique unit cell ($\gamma \neq 90°, 120°$),[54]

dx.doi.org/10.1021/jp4126792 | J. Phys. Chem. C 2014, 118, 7579−7590

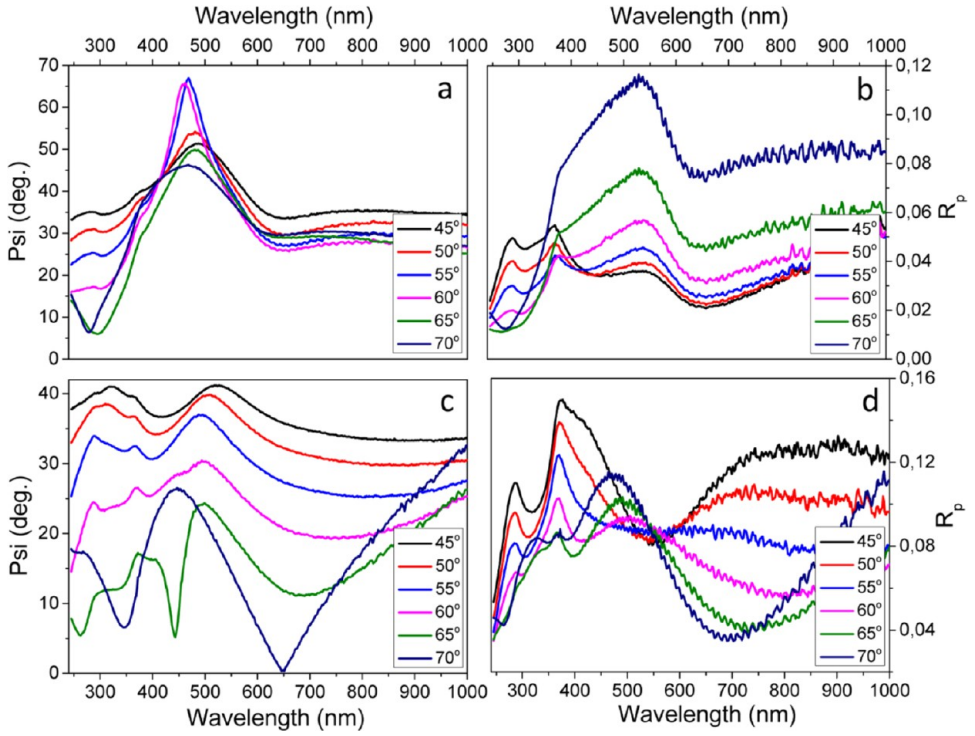

Figure 8. Optical properties of Au NP assemblies. Spectral dependences of ellipsometric parameter Ψ observed at 45−70° angles of incidence for Au NPs assembled on (a) Si/SiO_2 and (c) Si/TL_+ substrates. Measured p polarized reflectivity spectra as a function of incident angle, for Au NPs on (b) Si/SiO_2 and (d) Si/TL_+ substrates.

whereby the assemblies formed on the Si/TL_+ substrate better approximate the hexagonal symmetry. The different deviation from the hexagonal symmetry of the assemblies, deposited on different substrates, is reflected in the slightly different positions of the interference peaks, observed in the horizontal 1D cuts. The size of the coherent domains is comparable for the three samples and in the 100 ÷ 130 nm range. This evidence clearly indicates that Au NPs drop-cast on Si/SiO_2 substrate present a distorted hexagonal symmetry, reasonably induced by the low chemical affinity between the substrate surface and the NP capping molecules. An even larger distortion from the hexagonal symmetry was observed when the NPs were deposited on Si/TL_- substrates: in this case, the film swelling has a detrimental effect, as the chemical functionalization is lost and at the same time the very large structures formed hinder the NP regular organization on a flat substrate. However, Au NPs organize in a regular hexagonal symmetry when drop-cast on Si/TL_+ substrates due to the higher chemical affinity between the substrate surface and the NP capping molecules.

Finally, a preliminary investigation of the optical properties of the obtained Au NP assemblies was performed. First, the properties of Au NPs assembled on the Si/SiO_2 substrate were studied. The correlation between the features in ellipsometric and reflection spectra is shown in Figure 8a, b. In both cases, ellipsometric function Ψ and p polarized reflection spectra, peaks in the spectral region 450−550 nm of excitation LSPRs are present (Figure 8a, b). It is worth noticing that the resonance wavelength of the Au NPs on the Si/SiO_2 substrate (Figure 8a) demonstrate slightly red-shifted with respect to the value $\lambda \sim 525$ nm observed in solution (Figure 1b). Spectral position of resonances should be correlated with peaks in reflection spectra because the peaks observed for ellipsometric function Ψ are modified by dependence of s polarized reflectivity.

To determine the complex refractive index $N = n + ik$ of the deposited Au NPs, ellipsometric functions Ψ and Δ were experimentally measured and fitted using the Fresnel model. The extracted refractive indices n_x and k_x (in-plane of substrate) and n_z and k_z (out-of plane) for the studied Au NPs layer are shown in Figure S2a, b (Supporting Information). The obtained optical constants n_x and k_x unambiguously demonstrate resonances in the 400−450 nm and 550−650 nm wavelength ranges associated with LSPR of the Au NPs. For this region, the dependence of n_x and n_z shows abnormal dispersion while k_x and k_z reach the maximal values. The peaks in k_x and k_z in Figure S2a, b (Supporting Information) can be attributed to in-plane and out-plane plasmonic resonances parallel/perpendicular to the surface of the sample (x and z resonance).

Subsequently, the role of the substrate on the Au NP coupling was investigated. For this purpose, the optical properties of Au NPs deposited onto Si substrate functionalized with Teflon-like film with higher cross-linking degree (Si/TL_+) was investigated. Si/TL_+ substrate appears characterized by a quite flat and uniform surface with smaller average roughness in comparison to Si/SiO_2. The main features of ellipsometric Ψ and p polarized reflection R_p spectra for the Au NPs deposited on Si/TL_+ are shown in Figure 8c, d. The reflection spectra demonstrate a peak of the classical interference of the Fabry−Perot type joint with the prominent absorption peak of Si at wavelengths of ∼300−350 nm. In addition to these, a broad peak appears in all reflection curves R_p in the range 400−450 nm, which corresponds to the LSPR band (see Figure 8d). The resonance position of the R_p peak shows a strong angular dependence with the peak shifting to a shorter wavelength with

dx.doi.org/10.1021/jp4126792 | J. Phys. Chem. C 2014, 118, 7579−7590

the decrease of the angle of incidence of the probe light. The spectral position of the peak in Ψ and R_p is indeed related to the plasmon resonance of the Au NPs; however, its behavior is determined by the electromagnetic interaction between the resonances of the Au NPs and dipolar images in the substrate.[41,55] In particular, such interaction causes a blue shift of the mode, as the coupling between NPs changes due to presence of the Teflon-like layer. The results of the fitting of the ellipsometric function based on the Fresnel equations for anisotropic film (Figure 8c) are shown in Figure S2c, d (Supporting Information). The extracted optical constants clearly show the presence of LSPR at wavelengths 550−650 nm, which is blue-shifted of about 50 nm with respect to the LSPR position observed for the same Au NPs deposited on Si/SiO_2. Figure S2c (Supporting Information) shows an increase in the values for extracted real parts of refractive indexes n_x and n_z in the orange-red and near-infrared regions (above of 500 nm) and values both for k_x and k_z close to zero outside the LSPR region. The peaks in k_x and k_z (Figure S2c, d, Supporting Information) can be attributed to in-plane plasmonic resonances parallel (x resonance) and perpendicular (z resonance) to the surface of the sample, respectively. The experimental data show that z resonances are normally red-shifted with respect to x resonances for Au NPs deposited on Teflon-like functionalized Si substrates.

Interestingly, LSPRs are much wider for the NP assembly on Si/TL_+ substrate that is most probably due to stronger interactions between plasmonic resonance of individual NPs. In addition, it is worth pointing out that the observed LSPR z resonances are more intense for Au NPs deposited on silicon substrates. Finally, comparing Figure S2c, d (Supporting Information) with Figure S2a, b (Supporting Information), it is possible to conclude that the plasmonic properties of Au NPs strongly depend on the substrate, which influences NP ordering and near-field interactions between NPs.

CONCLUSIONS

In this work, a simple drop-casting procedure has demonstrated to be able to successfully fabricate 2D Au NP superlattice over hundreds of square micrometer areas. In particular, along with a suitable combination of NP dispersing solvent, evaporation temperature, and NP concentration, the role played by the surface chemistry of the substrate used for the deposition has been found decisive to achieve a uniform 2D NP organization hundreds of micrometers wide. Indeed, the ensemble of the experimental parameters has been established to influence the energetic contributions regulating the particle−particle interactions and the conditions required for NPs to reach their most energetically favorable position. In particular, the substrate chemistry that has been investigated by depositing Teflon-like films onto silicon, turning the surface from hydrophilic to hydrophobic. Optimization of the plasma process conditions for the deposition of the Teflon-like films has demonstrated crucial to achieve a resistant and effective coating. In fact, only the sample (Si/TL_+) deposited at higher power and monomer dilution in Ar, hence the more cross-linked, has been demonstrated to suit the specific experimental conditions. In addition, such a coating demonstrated particularly effective in directing a uniform 2D NP organization over hundreds of square micrometer areas. GISAXS experiments performed on Au NPs assembled onto the different substrates, at a given NP concentration, have confirmed the dependence of Au NP organization on the supporting substrate chemistry, showing that the only negligible deviation from the regular hexagonal symmetry can be found for the Si/TL_+ substrate. Spectroscopic ellipsometry investigation has clearly established that Au NPs assembled on Si/TL_+ substrate exhibit stronger interactions between plasmonic resonance of individual NPs, thus indicating that the plasmonic properties of the Au NP assemblies are strongly influenced by the substrate, which influences NP ordering and near-field interactions between NPs.

The reported results, while clearly confirming the viability of such a simple drop-casting procedure for fabrication and engineering of novel architectures based on NPs, unquestionably point out the role of surface chemistry to achieve for such assemblies the long-range order that is fundamental to fabricate materials interesting for its collective properties. Indeed, the fabricated Au NP based 2D structure can envisage a metamaterial where a strong transverse (intralayer) near-field coupling could also occur, deriving from the single NP component properties organized in the fabricated complex structure, thus resulting particularly effective for plasmonic applications. A limitation of the results reported on the control on Au NP assembly by depositing on substrates properly coated with Teflon-like film is that they lack accessibility for applications that require conductive substrates (e.g., photovoltaic, light emitting diodes, and microelectronics) due to the high resistivity of such coatings. However, it is worth pointing out that the main surface parameter crucial to drive the NP assembly, hence low wettability of the coating, could be effectively achieved using a different type of plasma treatment, able to perform fluorine surface grafting onto silicon, as well as onto other conductive substrate. In this way, it would be possible to accomplish the same surface characteristics, still keeping the substrate conductive properties and thus ultimately allowing the integration of such self-assembled structures into functional devices.

ASSOCIATED CONTENT

Supporting Information

SEM micrograph of the 2D Au NP assembly deposited on Si/TL_+ and Si/TL_- substrates, at different magnification; extracted optical constants of the Au NPs assembled on Si/SiO_2 and Si/TL_+ substrates. This material is available free of charge via the Internet at http://pubs.acs.org.

AUTHOR INFORMATION

Corresponding Author

*Phone: +39 (0)80 5442027; fax: +39 (0)80 5442128; e-mail: lucia.curri@ba.ipcf.cnr.it.

Notes

The authors declare no competing financial interest.

ACKNOWLEDGMENTS

This work was partially supported by the EU FP7 project "METACHEM" (grant agreement CP-FP 228762-2), by the SEED project "X-ray synchrotron class rotating anode microsource for the structural micro imaging of nanomaterials and engineered biotissues (XMI-LAB)"- IIT Protocol no. 21537 of 23/12/2009 and by Italian National Consortium for Material Science and Technology (INSTM). Rocco Lassandro is acknowledged for technical support.

REFERENCES

(1) Poznyak, S. K.; Talapin, D. V.; Shevchenko, E. V.; Weller, H. Quantum Dot Chemiluminescence. *Nano Lett.* **2004**, *4*, 693−698.

(2) Michalet, X.; Pinaud, F. F.; Bentolila, L. A.; Tsay, J. M.; Doose1, S.; Li, J. J.; Sundaresan, G.; Wu, A. M.; Gambhir, S. S.; Weiss, S. Quantum Dots for Live Cells, in Vivo Imaging, and Diagnostics. *Science* **2005**, *307*, 538−544.

(3) Chah, S.; Hammond, M.; Zare, R. N. Gold Nanoparticles as a Colorimetric Sensor for Protein Conformational Changes. *Chem. Biol.* **2005**, *12*, 323−328.

(4) Stevens, P. D.; Fan, J.; Gardimalla, H. M. R.; Yen, M.; Gao, Y. Superparamagnetic Nanoparticle-Supported Catalysis of Suzuki Cross-Coupling Reactions. *Org. Lett.* **2005**, *7*, 2085−2088.

(5) Petronella, F.; Fanizza, E.; Mascolo, G.; Locaputo, V.; Bertinetti, L.; Martra, G.; Coluccia, S.; Agostiano, A.; Curri, M. L.; Comparelli, R. Photocatalytic Activity of Nanocomposite Catalyst Films Based on Nanocrystalline Metal/Semiconductors. *J. Phys. Chem. C* **2011**, *115*, 12033−12040.

(6) Reineck, P.; Lee, G. P.; Brick, D.; Karg, M.; Mulvaney, P.; Bach, U. A Solid-State Plasmonic Solar Cell via Metal Nanoparticle Self-Assembly. *Adv. Mater.* **2012**, *24*, 4750−4755.

(7) Maria, A.; Cyr, P. W.; Klem, E. J. D.; Levina, L.; Sargent, E. H. Solution-Processed Infrared Photovoltaic Devices With >10% Monochromatic Internal Quantum Efficiency. *Appl. Phys. Lett.* **2005**, *87*, 213112.

(8) Correa-Duarte, M. A.; Grzelczak, M.; Salgueiriño-Maceira, V.; Giersig, M.; Liz-Marzán, L. M.; Farle, M.; Sierazdki, K.; Diaz, R. Alignment of Carbon Nanotubes under Low Magnetic Fields through Attachment of Magnetic Nanoparticles. *J. Phys. Chem. B* **2005**, *109*, 19060−19063.

(9) Hermanson, K. D.; Lumsdon, S. O.; Williams, J. P.; Kaler, E. W.; Velev, O. D. Dielectrophoretic Assembly of Electrically Functional Microwires from Nanoparticle Suspensions. *Science* **2001**, *294*, 1082−1086.

(10) Panine, P.; Narayanan, T.; Vermant, J.; Mewis, J. Structure and Rheology during Shear-Induced Crystallization of a Latex Suspension. *Phys. Rev. E: Stat. Phys., Plasmas, Fluids, Relat. Interdiscip. Top.* **2002**, *66*, 022401.

(11) Fanizza, E.; Malaquin, L.; Kraus, T.; Wolf, H.; Striccoli, M.; Micali, N.; Taurino, A.; Agostiano, A.; Curri, M. L. Precision Patterning with Luminescent Nanocrystal-Functionalized Beads. *Langmuir* **2010**, *26*, 14294−14300.

(12) Kershaw, S. V.; Sushaa, A. S.; Rogach, A. L. Narrow Bandgap Colloidal Metal Chalcogenide Quantum Dots: Synthetic Methods, Heterostructures, Assemblies, Electronic and Infrared Optical Properties. *Chem. Rev.* **2013**, *42*, 3033−3087.

(13) Shevchenko, E. V.; Talapin, D. V.; Murray, C. B.; O'Brien, S. Structural Characterization of Self-Assembled Multifunctional Binary Nanoparticle Superlattices. *J. Am. Chem. Soc.* **2006**, *128*, 3620−3637.

(14) Chen, J.; Dong, A.; Cai, J.; Ye, X.; Kang, Y.; Kikkawa, J. M.; Murray, C. B. Collective Dipolar Interactions in Self-Assembled Magnetic Binary Nanocrystal Superlattice Membranes. *Nano Lett.* **2010**, *10*, 5103−5108.

(15) Franzl, T.; Klar, T. A.; Schietinger, S.; Rogach, A. L.; Feldmann, J. Exciton Recycling in Graded Gap Nanocrystal Structures. *Nano Lett.* **2004**, *4*, 1599−1603.

(16) Corricelli, M.; Enrichi, F.; Altamura, D.; De Caro, L.; Giannini, C.; Falqui, A.; Agostiano, A.; Curri, M. L.; Striccoli, M. Near Infrared Emission from Monomodal and Bimodal PbS Nanocrystal Superlattices. *J. Phys. Chem. C* **2012**, *116*, 6143−6152.

(17) Kelly, K. L.; Coronado, E.; Zhao, L. L.; Schaz, G. C. The Optical Properties of Metal Nanoparticles: The Influence of Size, Shape, and Dielectric Environment. *J. Phys. Chem. B* **2003**, *107*, 668−677.

(18) Yang, S. C.; Kobori, H.; He, C. L.; Lin, M. H.; Chen, H. Y.; Li, C.; Kanehara, M.; Teranishi, T.; Gwo, S. Plasmon Hybridization in Individual Gold Nanocrystal Dimers: Direct Observation of Bright and Dark Modes. *Nano Lett.* **2010**, *10*, 632−637.

(19) Chen, H. Y.; He, C. L.; Wang, C. Y.; Lin, M. H.; Mitsui, D.; Eguchi, M.; Teranishi, T.; Gwo, S. Far-Field Optical Imaging of a Linear Array of Coupled Gold Nanocubes: Direct Visualization of Dark Plasmon Propagating Modes. *ACS Nano* **2011**, *5*, 8223−8229.

(20) Tao, A. R.; Sinsermsuksakul, P.; Yang, P. Tunable Plasmonic Lattices of Silver Nanocrystals. *Nat. Nanotechnol.* **2007**, *2*, 435−440.

(21) Tao, A. R.; Coperley, D. P.; Sinsermsuksakul, P.; Neureuther, A. R.; Yang, P. Self-Organized Silver Nanoparticles for Three-Dimensional Plasmonic Crystals. *Nano Lett.* **2008**, *8*, 4033−4038.

(22) Chen, C. F.; Tzeng, S. D.; Chenj, H. Y.; Lin, K. J.; Gwo, S. Tunable Plasmonic Response from Alkanethiolate-Stabilized Gold Nanoparticle Superlattices: Evidence of Near-Field Coupling. *J. Am. Chem. Soc.* **2008**, *130*, 824−826.

(23) Courty, A.; Mermet, A.; Albouy, P. A.; Duval, E.; Pileni, M. P. Vibrational Coherence of Self-Organized Silver Nanocrystals in f.c.c. Supra-Crystals. *Nat. Mater.* **2005**, *4*, 395−398.

(24) Dintinger, J.; Muehlig, S.; Rockstuhl, C.; Scharf, T. A Bottom-Up Approach to Fabricate Optical Metamaterials by Self-Assembled Metallic Nanoparticles. *Opt. Mater. Express* **2012**, *2*, 269−278.

(25) Liu, N.; Guo, H.; Fu, L.; Kaiser, S.; Schweizer, H.; Giessen, H. Three-Dimensional Photonic Metamaterials at Optical Frequencies. *Nat. Mater.* **2008**, *7*, 31−37.

(26) Enkrich, C.; Pérez-Willard, F.; Gerthsen, D.; Zhou, J.; Koschny, T.; Soukoulis, C. M.; Wegener, M.; Linden, S. Focused-Ion-Beam Nanofabrication of Near-Infrared Magnetic Metamaterials. *Adv. Mater.* **2005**, *17*, 2547−2549.

(27) Ditlbacher, H.; Hohenau, A.; Wagner, D.; Kreibig, U.; Rogers, M.; Hofer, F.; Aussenegg, F. R.; Krenn, J. R. Silver Nanowires as Surface Plasmon Resonators. *Phys. Rev. Lett.* **2005**, *95*, 257403.

(28) Halas, N. J.; Lal, S.; Chang, W.-S.; Link, S.; Nordlander, P. Plasmons in Strongly Coupled Metallic Nanostructures. *Chem. Rev.* **2011**, *111*, 3913−3961.

(29) Lin, M.-H.; Chen, H.-Y.; Gwo, S. Layer-by-Layer Assembly of Three-Dimensional Colloidal Supercrystals with Tunable Plasmonic Properties. *J. Am. Chem. Soc.* **2010**, *132*, 11259−11263.

(30) Zheng, N.; Fan, J.; Stucky, G. D. One-Step One-Phase Synthesis of Monodisperse Noble-Metallic Nanoparticles and Their Colloidal Crystals. *J. Am. Chem. Soc.* **2006**, *128*, 6550−6551.

(31) Lin, X. M.; Jaeger, H. M.; Sorensen, C. M.; Klabunde, K. J. Formation of Long-Range-Ordered Nanocrystal Superlattices on Silicon Nitride Substrates. *J. Phys. Chem. B* **2001**, *105*, 3353−3357.

(32) Eah, S.-K. A Very Large Two-Dimensional Superlattice Domain of Monodisperse Gold Nanoparticles by Self-Assembly. *J. Mater. Chem.* **2011**, *21*, 16866−16868.

(33) Liao, J.; Mangold, M. A.; Grunder, S.; Mayor, M.; Schönenberger, C.; Calame, M. Interlinking Au Nanoparticles in 2D Arrays Via Conjugated Dithiolated Molecules. *New J. Phys.* **2008**, *10*, 065019.

(34) Mangold, M. A.; Niedermeier, M. A.; Rawolle, M.; Dirks, B.; Perlich, J.; Roth, S. V.; Holleitner, A. W.; Müller-Buschbaum, P. Correlation between Structure and Optoelectronic Properties in a Two-Dimensional Nanoparticle Assembly. *Phys. Status Solidi RRL* **2011**, *5*, 16−18.

(35) Hiramatsu, H.; Osterloh, F. E. A Simple Large-Scale Synthesis of Nearly Monodisperse Gold and Silver Nanoparticles with Adjustable Sizes and with Exchangeable Surfactants. *Chem. Mater.* **2004**, *16*, 2509−2511.

(36) Fanizza, E.; Depalo, N.; Clary, L.; Agostiano, A.; Striccoli, M.; Curri, M. L. A Combined Size Sorting Strategy for Monodisperse Plasmonic Nanostructures. *Nanoscale* **2013**, *5*, 3272−3282.

(37) Liu, X.; Atwater, M.; Wang, J.; Huo, Q. Extinction Coefficient of Gold Nanoparticles with Different Sizes and Different Capping Ligands. *Colloids Surf., B* **2007**, *58*, 3−7.

(38) D'Agostino, R.; Cramarossa, F.; Fracassi, F.; Illuzzi, F. In *Plasma Deposition, Treatment and Etching of Polymers*; D'Agostino, R., Ed.; Academic Press: Boston, MA, 1990; p 95.

(39) Milella, A.; Palumbo, F.; D'Agostino, R. In *Advanced Plasma Technology*; D'Agostino, R., Favia, P., Kawai, Y., Ikegami, H., Sato, N., Arefi-Khonsari, F., Eds.; WILEY-VCH: Weinheim, Germany, 2008; p 175.

(40) Altamura, D.; Lassandro, R.; Vittoria, F. A.; De Caro, L.; Siliqi, D.; Ladisa, M.; Giannini, C. X-Ray Microimaging Laboratory (XMI-LAB). *J. Appl. Crystallogr.* **2012**, *45*, 869−873.
(41) Kravets, V. G.; Schedin, F.; Taylor, S.; Viita, D.; Grigorenko, A. N. Plasmonic Resonances in Optomagnetic Metamaterials Based on Double Dot Arrays. *Opt. Express* **2010**, *18*, 9780−9790.
(42) Miller, M. M.; Lazarides, A. A. Sensitivity of Metal Nanoparticle Surface Plasmon Resonance to the Dielectric Environment. *J. Phys. Chem. B* **2005**, *109*, 21556−21565.
(43) Corricelli, M.; Altamura, D.; De Caro, L.; Guagliardi, A.; Falqui, A.; Genovese, A.; Agostiano, A.; Giannini, C.; Striccoli, M.; Curri, M. L. Self-Organization of Mono- and Bi-Modal PbS Nanocrystal Populations in Superlattices. *CrystEngComm* **2011**, *13*, 3988−3997.
(44) Murray, C. B.; Kagan, C. R.; Bawendi, M. G. Synthesis and Characterization of Monodisperse Nanocrystals and Close-Packed Nanocrystal Assemblies. *Annu. Rev. Mater. Sci.* **2000**, *30*, 545−610.
(45) Fini, P.; Depalo, N.; Comparelli, R.; Curri, M. L.; Striccoli, M.; Castagnolo, M.; Agostiano, A. Interactions between Surfactant Capped CdS Nanocrystals and Organic Solvent. *J. Therm. Anal. Calorim.* **2008**, *92*, 271−277.
(46) Lide, D. R. *Handbook of Organic Solvents*; CRC Press: Boca Raton, FL, 1994.
(47) Garbassi, F.; Morra, M.; Occhiello, E. *Polymer Surfaces, From Physics to Technology*; John Wiley and Sons: Chichester, U.K.; 1994.
(48) Extrand, C. W.; Kumagai, Y. An Experimental Study of Contact Angle Hysteresis. *J. Colloid Interface Sci.* **1997**, *191*, 378−383.
(49) Young, T. An Essay on the Cohesion of Fluids. *Philos. Trans. R. Soc. London* **1805**, *95*, 65−87.
(50) Lazzari, R. IsGISAXS: A Program for Grazing-Incidence Small-Angle X-Ray Scattering Analysis of Supported Islands. *J. Appl. Crystallogr.* **2002**, *35*, 406−421.
(51) Renaud, G.; Lazzari, R.; Leroy, F. Probing Surface and Interface Morphology with Grazing Incidence Small Angle X-Ray Scattering. *Surf. Sci. Rep.* **2009**, *64*, 255−380.
(52) Altamura, D.; Sibillano, T.; Siliqi, D.; De Caro, L.; Giannini, C. Assembled Nanostructured Architectures Studied by Grazing Incidence X-Ray Scattering. *Nanomater. Nanotechnol.* **2012**, *2*, 16.
(53) Lazzari, R.; Leroy, F.; Renaud, G. Grazing-Incidence Small-Angle X-Ray Scattering from Dense Packing of Islands on Surfaces: Development of Distorted Wave Born Approximation and Correlation between Particle Sizes and Spacing. *Phys. Rev. B: Condens. Matter Mater. Phys.* **2007**, *76*, 125411.
(54) Giacovazzo, C.; Monaco, H. L.; Viterbo, D.; Scorari, F.; Gilli, G.; Zanotti, G.; Catti, M. *Fundamentals of Crystallography*; Oxford University Press: New York, 1994; Chapter 1, pp 18−19.
(55) Yamaguchi, T.; Yoshida, S.; Kinbara, A. Optical Effect of the Substrate on the Anomalous Absorption of Aggregated Silver Films. *Thin Solid Films* **1974**, *21*, 173−187.